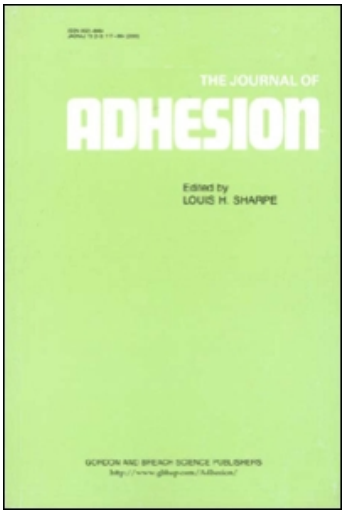

The Journal of Adhesion
Publication details, including instructions for authors and subscription information:
http://www.informaworld.com/smpp/title~content=t713453635

Surface Energy Analysis of Carbon Fibers and Films

P. J. Dynes[a]; D. H. Kaelble[a]
[a] Science Center. Rockwell International, Thousand Oaks, California, U.S.A.

To cite this Article Dynes, P. J. and Kaelble, D. H.(1974) 'Surface Energy Analysis of Carbon Fibers and Films', The Journal of Adhesion, 6: 3, 195 — 206
To link to this Article: DOI: 10.1080/00218467408075026
URL: http://dx.doi.org/10.1080/00218467408075026

J. Adhesion, 1974, Vol. 6, pp. 195–206

Printed in Scotland

Surface Energy Analysis of Carbon Fibers and Films

P. J. DYNES and D. H. KAELBLE

Science Center, Rockwell International, Thousand Oaks, California 91360, U.S.A.

(*Received June 25, 1973*)

Amorphous and graphitic carbon fibers and film surfaces are characterized by wettability measurements and surface energy analysis which isolate the (London-*d*) dispersion γ_{SV}^d and (Keesom-*p*) polar γ_{SV}^p contribution to solid–vapor surface tension $\gamma_{SV} = \gamma_{SV}^d + \gamma_{SV}^p$. Graphitized carbon fibers which are surface treated to provide strong bonding to polar matrix resins show consistent strong polar contributions to total surface tension with $\gamma_{SV}^d/\gamma_{SV} \simeq \gamma_{SV}^p/\gamma_{SV} \simeq 0.50$. Amorphous carbon films prepared for biological implant applications display dominant dispersion character in surface energy with $\gamma_{SV}^d/\gamma_{SV} \simeq 0.74$ to 0.95 and $\gamma_{SV}^p/\gamma_{SV} \simeq 0.05$ to 0.24.

INTRODUCTION

Interest in amorphous and graphitic carbon is high at the present time due to its use as a reinforcement in advanced composite materials[1] and as a thrombo-resistant material for prosthetic implant devices.[2] In both of these applications surface properties play an important role in performance and reliability. In order to understand more clearly this critical surface zone, we have carried out wettability studies on two graphitic types of composite reinforcements and two amorphous carbon implant materials.

The two advanced composite reinforcements studied were Union Carbide Thornel 400 graphite fiber and Pfizer pyrolytic graphite ribbon. Thornel 400 graphite fiber is produced by graphitization of a polyacrylonitrile precusor. The Pfizer product is a thin flexible film produced by vapor deposition of carbon on a hot surface. Unlike the unidirectional strength and modulus properties of graphite fibers, the graphite ribbon is reported[3] to display isotropy in the two dimensions of the film plane.

The two implant materials examined are products of Gulf Energy and Environmental Systems, Inc. One is vapor deposited silicon alloyed Pyrolite®

carbon which has been diamond polished. The second is a vapor deposited carbon on a polymeric substrate.

EXPERIMENTAL

A summary of the results of *advancing* contact angle measurements are furnished in Table I. Included are contact angle values reported by Baier[2] for a diamond polished carbon surface used in implant studies. Contact angle results for Thornel 400 graphite fibers presented in Table I were determined by the single fiber micro Wilhelmy plate technique.[4, 5] Contact

TABLE I

Cosine of advancing liquid–solid contact angles θ of test liquids on various carbon surfaces

Test liquid	γ_{LV} (dyn/cm)	ΔM (μgm)	Thornel 400 graphite fibers cos θ	Pfizer graphite ribbon cos θ	Gulf vapor deposited carbon cos θ	Gulf diamond polished carbon cos θ	Baier's diamond polished carbon (Ref. 2) cos θ
Water	72.8	144	0.734	0.105	0.301	0.087	0.17
Glycerol	64.0	173	1.00	0.857	0.751	0.225	0.64
Formamide	58.3	118	0.749	0.438	0.676	0.454	0.60
Ethylene glycol	48.3	124	0.950	0.574	0.629	0.588	—
Tricresyl phosphate	40.9	104	0.941	0.891	0.949	0.982	—
Poly glycol P–1200	31.3	84.3	1.00	0.914	0.956	0.984	—
Poly glycol E–200	43.5	—	—	0.755	0.821	0.788	—
Poly glycol 15–200	36.6	94.1	0.951	0.839	0.857	0.974	—
1-Bromonaphthalene	44.6	111	0.921	0.982	0.956	0.966	—
Hexadecane	27.6	70.0	0.938	0.999	0.990	0.998	—
Methylene iodide	50.8	—	—	—	—	—	0.99
Hexane	18.4	47.0	0.945	—	—	—	—

angle measurements on the other surfaces were made by the sessile drop method at 20°C in the B-100 Environmental Chamber of the NRL goniometer (Rame-Hart Inc.). The test liquids used in the present study are listed in Table II in descending order of surface tension values. Several techniques, including platinum–iridium Wilhelmy plate, glass capillary rise, and DuNouy ring method were used to determine the surface tension of the test liquids. Agreement between experimental and literature values of liquid surface tension, generally within ± 0.5 dyn/cm, is taken as evidence of purity.

TABLE II
Surface tension properties of test liquids at 20°C

Test liquid	γ_{LV}	γ_{LV}^{d} dyn/cm	γ_{LV}^{p}	$2\alpha_L$ (dyn/cm)$^{\frac{1}{2}}$	β_L/α_L
Water	72.8	21.8	51.0	9.34	1.53
Glycerol	64.0	34.0	30.0	11.66	0.94
Formamide	58.3	32.3	26.0	11.37	0.90
Diiodomethane	50.8	48.5	2.3	13.93	0.22
Ethylene glycol	48.3	29.3	19.0	10.83	0.81
1-Bromonapthalene	44.6	44.6	0.0	13.36	0.00
Glycol PG-E-1200	43.5	28.2	15.3	10.62	0.74
Tricresyl phosphate	40.9	39.2	1.7	12.52	0.21
Glycol PG-15-200	36.6	26.0	10.6	10.20	0.64
Glycol PG-P-1200	31.3	24.5	6.8	9.90	0.53
n-Hexadecane	27.6	27.6	0.0	10.51	0.00
Ethanol (abs.)	22.4	17.0	5.4	8.24	0.56
Hexane	18.4	18.4	0.0	8.58	0.00

The surfaces studied in the present report were used as received from the manufacturer, except for the Thornel 400 graphite fiber and Gulf vapor deposited carbon. These were rinsed in absolute ethanol and dried between measurements with the various test liquids. In addition, the Thornel 400

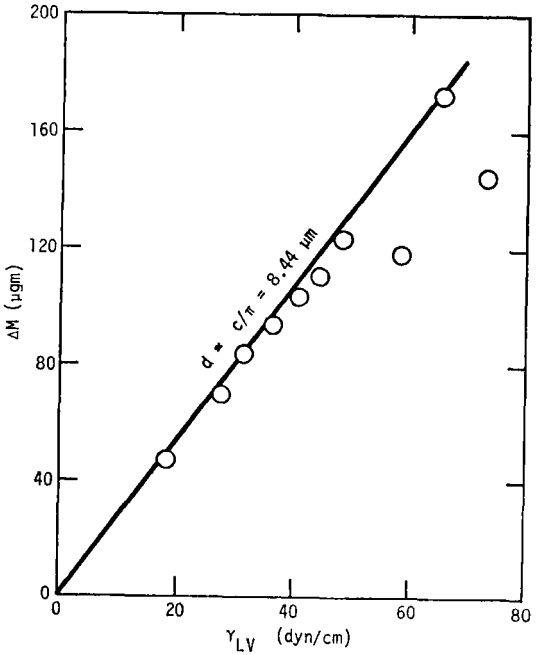

FIGURE 1 Fiber–liquid contact force ΔM versus liquid surface tension γ_{LV} Thornel 400 graphite fiber.

graphite fiber was washed several times in acetone prior to its study to remove the polyvinyl alcohol sizing.

Using the Wilhelmy plate technique the contact force ΔM (μgm) between a single fiber of circumference C and a liquid of surface tension γ_{LV} is described by the following relation[4, 5]

$$\Delta M = \frac{C\gamma_{LV} \cos\theta}{g} \tag{1}$$

where θ is the advancing liquid–solid contact angle and $g = 980.6$ dyn/cm. By this relation both fiber circumference and advancing contact angle can be determined. In Figure 1 contact force ΔM (μgm) as measured by a recording

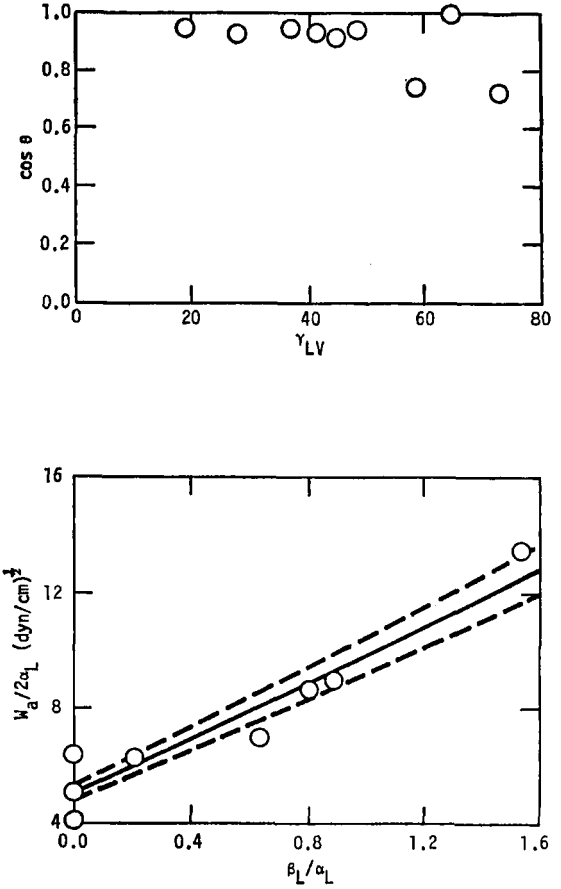

FIGURE 2 Critical surface tension plot (upper portion) and $W_a/2\alpha_L$ versus β_L/α_L for Thornel 400 graphite fiber.

Cahn electrobalance is plotted versus liquid surface tension γ_{LV}. The curve drawn in Figure 1 corresponds to that for maximum wetting ($\cos\theta = 1.0$), thus allowing calculation of fiber circumference in Eq. (1). From this circumference an apparent diameter $d \simeq C/\pi$ can be calculated which corresponds closely with that revealed by microscopic examination. Those points which lie below the curve in Figure 1 represent liquids whose contact angles are

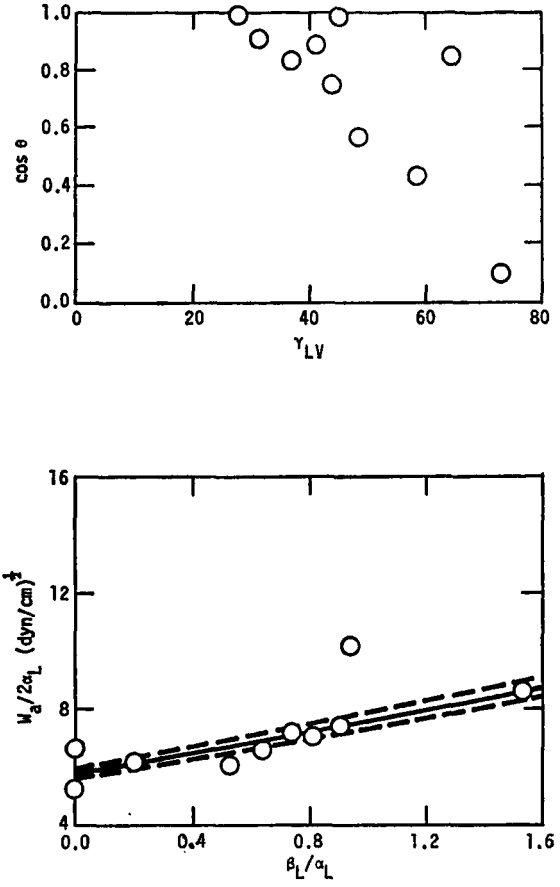

FIGURE 3 Critical surface tension plot (upper portion) and $W_a/2\alpha_L$ versus β_L/α_L for Pfizer graphite ribbon.

greater than zero on the fiber surface. It was found that contact angle values for water on the carbon surfaces decreased substantially with time after a few minutes but that those for the other test liquids showed very little change. In order to overcome this problem only the initial contact angles measured

within a few seconds after contact of the water with the surface are given in Table I.

In the upper portions of Figures 2 through 6 the wetting data are presented in a plot of cos θ versus γ_{LV}. As discussed by Zisman and coworkers[6] a critical

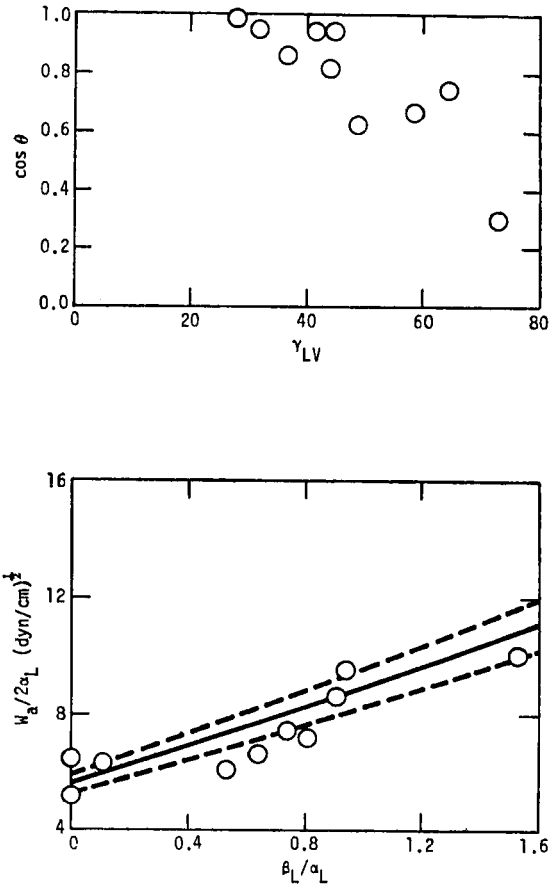

FIGURE 4 Critical surface tension plot (upper portion) and $W_a/2\alpha_L$ versus β_L/α_L for Gulf vapor deposited carbon.

surface tension γ_C for the solid surface is obtained from such a linear plot of cos θ versus γ_{LV} if an extrapolation to cos $\theta = 1.0$ is made. For the test liquid series used in the present study the critical surface tension plots in the upper portions of Figures 2 through 5 show a large amount of data scatter. In Figure 6 from work by Baier[2] the critical surface tension plot for a diamond polished carbon material shows a high $\gamma_C \simeq 50$ dyn/cm. In order to obtain

a more accurate description of the wetting behavior of these solid surfaces we have further analyzed the data by a two parameter model for interfacial interactions discussed by Kaelble.[7]

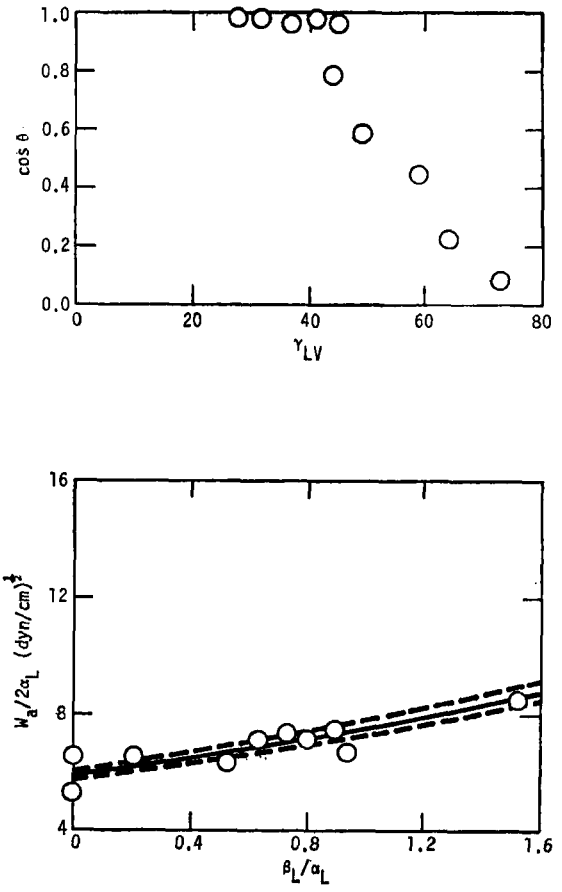

FIGURE 5 Critical surface tension plot (upper portion) and $W_a/2\alpha_L$ versus β_L/α_L for Gulf diamond polished carbon.

SURFACE ENERGY ANALYSIS

In the analysis the surface energies of solids and liquids are considered to be the sum of separate (London-*d*) dispersion and (Keesom-*p*) polar contributions. From such a two component model the following relations can be

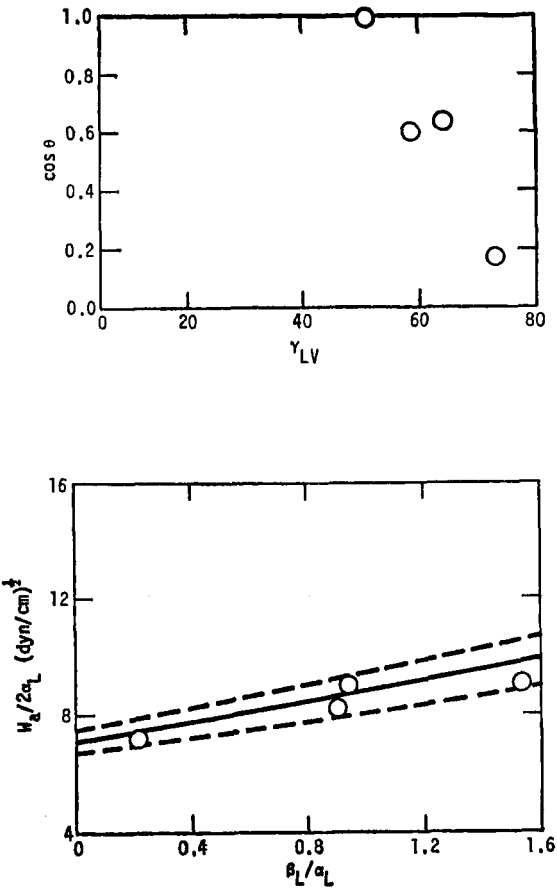

FIGURE 6 Critical surface tension plot (upper portion) and $W_a/2\alpha_L$ versus β_L/α_L for Baier's diamond polished carbon (Ref. 2).

derived for the polar and dispersion interactions between liquids and solids.[7]

$$\gamma_{LV} = \gamma_{LV}^d + \gamma_{LV}^p = \alpha_L^2 + \beta_L^2 \tag{2}$$

$$\gamma_{SV} = \gamma_{SV}^d + \gamma_{SV}^p = \alpha_S^2 + \beta_S^2 \tag{3}$$

$$W_a = \gamma_{LV}(1 + \cos\theta) \leqslant 2\gamma_{LV} \tag{4}$$

$$W_a = 2[\alpha_L\alpha_S + \beta_L\beta_S] = W_a^d + W_a^p \tag{5}$$

$$\frac{W_a}{2\alpha_L} = \alpha_S + \beta_S(\beta_L/\alpha_L) \tag{6}$$

where

γ_{LV} = liquid–vapour surface tension

γ_{SV} = solid–vapour surface tension

α_L, β_L = square root of the respective (London) dispersion γ^d_{LV} and (Keesom) polar γ^p_{LV} parts of γ_{LV}

α_S, β_S = square roots of respective dispersion γ^d_{SV} and polar γ^p_{SV} parts of γ_{SV}

W_a = nominal work of adhesion

θ = liquid–solid contact angle

By this technique values for nominal works of adhesion determined from Eq. (4) are substituted into Eq. (6) where α_L and β_L are calculated from the literature values of γ^d_{LV} and γ^p_{LV} as given in Table II. In Eq. (6) a linear function of $W_a/2\alpha_L$ versus β_L/α_L is predicted whose intercept at $\beta_L/\alpha_L = 0$ is $\alpha_S = (\gamma^d_{SV})^{\frac{1}{2}}$ and whose slope is $\beta_S = (\gamma^p_{SV})^{\frac{1}{2}}$. Table III presents the data in the form for graphical analysis described by Eq. (6). The lower portions of Figures 2 through 6 show these data plotted according to Eq. (7). The solid and dashed lines in these figures represent the calculated values of γ^d_{SV} and γ^p_{SV} with their respective standard deviations δ^d and δ^p as calculated by a determinant method of analysis.[8] Table IV summarizes the results obtained for all the surfaces studied including analysis of Baier's data[2] for a diamond polished carbon and four additional types of graphite fibers previously reported.[7]

TABLE III

Analysis of liquid–solid interactions

γ_L dyn/cm	$2\alpha_L$ (dyn/cm)$^{\frac{1}{2}}$	β_L/α_L	Thornel 400 graphite fiber $W_a/2\alpha_L$ (dyn/cm)$^{\frac{1}{2}}$	Pfizer graphite ribbon $W_a/2\alpha_L$ (dyn/cm)$^{\frac{1}{2}}$	Gulf vapor deposited carbon $W_a/2\alpha_L$ (dyn/cm)$^{\frac{1}{2}}$	Gulf diamond polished carbon $W_a/2\alpha_L$ (dyn/cm)$^{\frac{1}{2}}$	Diamond polished carbon (Ref. 1) $W_a/2\alpha_L$ (dyn/cm)$^{\frac{1}{2}}$
72.8	9.34	1.53	13.5	8.61	10.14	8.47	9.15
64.0	11.66	0.94	—	10.19	9.61	6.72	9.02
58.3	11.37	0.90	8.97	7.38	8.59	7.46	8.21
48.3	10.83	0.81	8.70	7.02	7.27	7.08	—
40.9	12.52	0.21	6.34	6.18	6.37	6.47	—
31.3	9.90	0.53	—	6.05	6.18	6.27	—
43.5	10.62	0.74	—	7.19	7.46	7.32	—
36.6	10.20	0.64	7.00	6.60	6.66	7.08	—
44.6	13.36	0.00	6.41	6.62	6.53	6.56	—
27.6	10.51	0.00	5.09	5.25	5.23	5.25	—
50.8	13.93	0.22	—	—	—	—	7.26
18.4	8.58	0.00	4.17	—	—	—	—

DISCUSSION OF RESULTS

One result which is immediately evident from the analysis is that the graphite fibers all show a high polar component of $\gamma_{SV}^{p} \sim 28$ dyn/cm compared to $\gamma_{SV}^{p} \sim 2$ to 11 dyn/cm for the other carbon surfaces.

One possible consequence of this high polar component found for the graphite surface energy is that in composite materials made with such fibers the fiber/matrix interface would be sensitive to moisture exposure. A recent

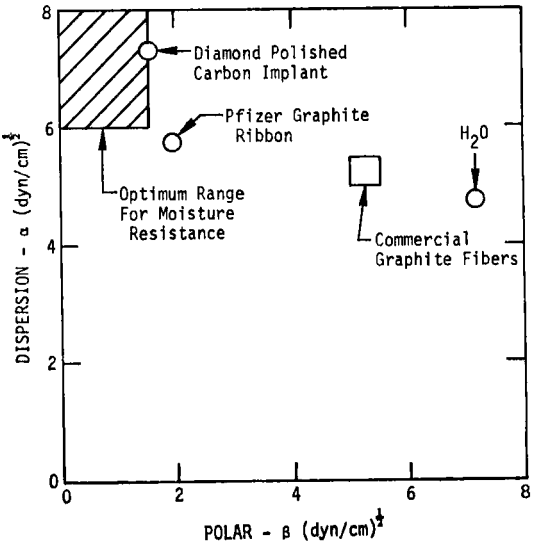

FIGURE 7 Dispersion surface energy component α versus polar component β for composite reinforcement materials. Shaded area indicates optimum zone for moisture insensitivity.

study[9] has shown that a substantial reduction in mechanical fracture energy does occur under high humidity or water immersion at 100°C for a graphite fiber/epoxy matrix composite. This reduction in fracture energy is believed to be a result of degradation of interfacial contributions to the total fracture energy. In Figure 7 a plot of $\alpha = (\gamma_{SV}^{d})^{\frac{1}{2}}$ versus $\beta = (\gamma_{SV}^{p})^{\frac{1}{2}}$ is presented for the composite reinforcement carbon surfaces. All the graphite fibers display values within a small range of $\alpha \simeq \beta \simeq 5.3$ (dyn/cm)$^{\frac{1}{2}}$. In order to overcome moisture sensitivity at the fiber/matrix interface, it has been suggested[9] that fiber surface energies should ideally lie in the shaded zone in Figure 7 where $\alpha_S \geqslant 6.0$ (dyn/cm)$^{\frac{1}{2}}$ and $\beta_S \leqslant 1.5$ (dyn/cm)$^{\frac{1}{2}}$. Within this zone the high dispersion surface energy should compensate for the decreased polar component to provide a strong, yet relatively moisture insensitive interfacial bond.

The Pfizer graphite ribbon in this respect displays values much closer to the optimum region indicated than do virgin graphite fibers.

Results of the analysis for the amorphous carbon implant materials given in Table IV show them to have relatively nonpolar surfaces compared to the graphite fibers. Baier's diamond polished carbon surface, although showing a low polar component ($\gamma_{SV}^{p} = 2.4$ dyn/cm), does differ from the two Gulf implant materials in having a much higher dispersion component ($\gamma_{SV}^{d} = 53.3$ dyn/cm).

Recently Baier[10] has suggested that on a critical surface tension plot of $\cos\theta$ versus γ_{LV} there exists a zone of maximum thromboresistance (or minimum cell spreading) defined by a range of critical surface tension values $23 \leqslant \gamma_c \leqslant 28$ dyn/cm at $\cos\theta = 1.0$ and slope factors $b = (-d\cos\theta/d\gamma_{LV})$ of $0.016 \leqslant b \leqslant 0.026$ (cm/dyne) for the linear plots. We are currently proceeding to apply the two-parameter dispersion-polar argument to more clearly define such a zone and to the analysis of available wettability data on biologically important materials.

TABLE IV

Summary of solid surface tension properties

	$\gamma_{SV}^{d} \pm \delta^{d}$ (dyn/cm)	$\gamma_{SV}^{p} \pm \delta^{d}$ (dyn/cm)	$\gamma_{SV} \pm \delta$ (dyn/cm)
Hercules HT-S® (Ref. 7)	25.9±1.5	25.7±3.3	51.6±2.3
Hercules HM-S® (Ref. 7)	26.1±2.1	26.8±4.1	52.8±2.7
Morganite II® (Ref. 7)	27.4±1.6	27.3±4.1	54.7±3.1
Modmor II® (Ref. 7)	28.3±3.5	29.4±6.0	58.2±2.8
Thornel® 400 graphite fiber	25.5±2.6	23.4±3.6	49.0±1.8
Pfizer graphite ribbon	33.0±1.6	3.6±0.6	36.6±1.1
Gulf vapor deposited carbon	32.2±2.6	11.3±2.7	43.4±2.1
Gulf diamond polished pyrolite® carbon	34.5±1.5	3.2±0.5	37.6±1.0
Baier's diamond polished carbon (Ref. 2)	53.3±6.1	2.4±1.0	55.8±5.4

® = Trademark

CONCLUSIONS

This study shows that graphitized carbon fibers which have been surface treated to provide strong bonding to polar matrix resins show consistent strong polar contributions to total surface tension with $\gamma_{SV}^{d}/\gamma_{SV} \simeq \gamma^{p}/\gamma_{SV} \simeq 0.50$. Amorphous carbon films prepared for biological implant applications display dominant dispersion character in surface energy with $\gamma_{SV}^{d}/\gamma_{SV} \simeq 0.74$

to 0.95 and $\gamma_{SV}^{p}/\gamma_{SV} \simeq 0.05$ to 0.24. The two parameter models for surface energy analysis utilized in this discussion appears to provide a new and useful approach to isolating the dispersion and polar mechanisms of interfacial bonding in biologically important materials. A system of analysis has been developed[7-9] which utilizes the results of surface energy analysis for γ_{SV}^{d} and γ_{SV}^{p} to predict the effect of adverse immersion environments upon fracture energy and strength of bonded interfaces. This analysis scheme has recently been successfully exploited in reinforced composite systems[9] and preliminary investigations strongly suggest its capability in analyzing adhesion phenomena in biological systems.

Acknowledgements

Thanks are expressed to Dr. R. W. Froberg of Pfizer Inc., and Drs. J. C. Bokros and F. J. Schoen of Gulf General Atomic Company for their generous donation of samples used in the present study. This work was supported in part by the Rockwell International IR & D Interdivisional Technology Program under the sponsorship of the Composites Technical Panel.

References

1. D. A. Scola and S. C. Brooks, *J. Adhesion* **2**, 213 (1970).
2. R. E. Baier, V. L. Gott, and A. Feruse, *Trans. Amer. Soc. Artif. Int. Organs* **16**, 50 (1970).
3. *Chem. and Eng. News*, July 19, 1971, p. 14.
4. A. W. Neuman and W. Tanner, *Proc. 5th Int. Cong. on Surface Activity* **2**, 727–734 (1968).
5. G. Mozzo and R. Chabord, Proc. 23rd Annual Conf., Reinforced Plastics/Composites Division, Soc. Plastics Industry, Section 9–C (1968), pp. 1–8.
6. W. A. Zisman, in *Adhesion and Cohesion* P. Weiss, Editor (Elsevier, Amsterdam, 1962). P. 176.
7. D. H. Kaelble, *Proc. 23rd Int. Cong. of Pure and Applied Chem.* **8**, 265 (1971).
8. D. H. Kaelble, *Physical Chemistry of Adhesion* (Wiley–Interscience, New York, 1971).
9. D. H. Kaelble, P. J. Dynes, and E. H. Cirlin, Symposium on Interfacial Bonding and Fracture in Polymeric, Metallic, and Ceramic Composites, Univ. Cal., Los Angeles, Nov. 1972 (to be published in *J. Adhesion*).
10. R. E. Baier, in Adhesion in Biological Systems, R. S. Manly, Editor (Academic Press, New York, 1970). Chap. 2.